DEMONSTRATION OF A BALLOON BORNE ARC-SECOND POINTER DESIGN

Keith D. DeWeese[(1)], Philip R. Ward[(2)]

[(1)] NASA Goddard Space Flight Center, Code 595, Greenbelt, MD 20771, USA, Email: keith.d.deweese@nasa.gov
[(2)] NASA Wallops Flight Facility, Code 598, Wallops Island, VA 23337, USA, Email: philip.r.ward@nasa.gov

ABSTRACT

Many designs for utilizing stratospheric balloons as low-cost platforms on which to conduct space science experiments have been proposed throughout the years. A major hurdle in extending the range of experiments for which these vehicles are useful has been the imposition of the gondola dynamics on the accuracy with which an instrument can be kept pointed at a celestial target. A significant number of scientists have sought the ability to point their instruments with jitter in the arc-second range. This paper presents the design and analysis of a stratospheric balloon borne pointing system that is able to meet this requirement. The test results of a demonstration prototype of the design with similar ability are also presented.

Discussion of a high fidelity controller simulation for design analysis is presented. The flexibility of the flight train is represented through generalized modal analysis. A multiple controller scheme is utilized for coarse and fine pointing. Coarse azimuth pointing is accomplished by an established pointing system, with extensive flight history, residing above the gondola structure. A pitch-yaw gimbal mount is used for fine pointing, providing orthogonal axes when nominally on target. Fine pointing actuation is from direct drive dc motors, eliminating backlash problems. An analysis of friction nonlinearities and a demonstration of the necessity in eliminating static friction are provided. A unique bearing hub design is introduced that eliminates static friction from the system dynamics. A control scheme involving linear accelerometers for enhanced disturbance rejection is also presented. Results from a linear analysis of the total system and the high fidelity simulation are given.

Results from a generalized demonstration prototype are presented. Commercial off-the-shelf (COTS) hardware was used to demonstrate the efficacy and performance of the pointer design for a mock instrument. Sub-arcsecond pointing ability from a ground hang test setup is shown from the testing results.

This paper establishes that the proposed control strategy can be made robustly stable with significant design margins. Also demonstrated is the efficacy of the proposed system in rejecting disturbances larger than those considered realistic. The system is implemented and demonstrates sub arc second pointing ability using COTS hardware. Finally, we see that sub arc-second pointing stability can be achieved for a large instrument pointing at an inertial target.

1 BACKGROUND

NASA's Scientific Balloon Program affords researchers the opportunity to conduct research in a near-space environment. Flight altitudes of 120k feet are typical, which place the balloons above more than 99½% of the earth's atmosphere [1]. This naturally makes them attractive platforms on which to mount space-viewing telescopes.

In order to successfully utilize balloons as platforms for telescopes, a means of pointing the instrument at the intended target within the required accuracy and jitter limits is necessary. Various pointing systems have been utilized or proposed. Thus far, none has demonstrated jitter less than several arcseconds. There is widespread interest among potential investigators for pointing excursions less than one arcsecond.

This paper discusses a balloon borne pointing system that can achieve sub-arcsecond stability of a balloon borne telescope viewing a celestial target. We begin with discussion of the salient design requirements, dynamic phenomena, and engineering considerations. Next a description of the system synthesized to address these for a straw man telescope is presented; the rationale for each of the design choices is included. A presentation and discussion of the results of comprehensive system analyses is then presented. Finally, we conclude with actual test results from an assembled demonstration prototype of the system.

2 DESIGN CONSIDERATIONS

For purposes of this study it was assumed that the instrument is a 3 ft (0.91 m) diameter, 24 ft (7.32 m) long telescope pointing at a celestial target. Weight is assumed to be 1500 lb (680 kg). Moments-of-inertia (MOI) are derived assuming uniform weight distribution in a thin wall cylinder which results in MOIs of 2230 sl-ft^2 (3023 kg-m^2) and 105 sl-ft^2 (142 kg-m^2) about the transverse and longitudinal axes respectively.

It is assumed that the instrument will be operating at night over long viewing durations. This implies that sufficient energy to operate the pointing system for several hours each day will have to be stored on-board. It is also assumed that the system will be operated every day for several weeks. From a practical standpoint, this implies that the energy required for operation will need to be replenished during daylight hours via solar panels. Consequently, this leads to the conclusion that the energy form be electrical and the quantity required kept to a minimum.

Maintaining sub-arcsecond pointing at an inertial target is principally a disturbance rejection problem rather than a target-tracking problem. This leads to the important conclusion that the magnitude of the actuator torques will be driven by the magnitudes of the disturbances and not the inertia of the telescope. Minimization of corrective torques is facilitated by early detection of disturbances.

One should recognize that perfect balance of the telescope in its mounting will never be achieved. Consequently, a secular body fixed moment will be present which the control system will have to compensate with a secular actuator torque. If corrective torques are provided by momentum wheels, they will be quickly saturated. If mass expulsion is used (e.g., cold gas), it will be rapidly exhausted.

Of paramount importance is the elimination of the deleterious effects of system non-linearities. Of special concern is static friction in the telescope mount. This will invariably result in limit cycling, the magnitude of which will almost certainly exceed one arcsecond.

Strength requirements are levied on the system to ensure that no part is separated from the gondola during parachute deployment. Among these requirements is the ability to survive a 10g load.

The quality of the sensor data is going to create an absolute limit of performance that any system can attain. The principal question this study seeks to address is how tightly the inertial attitude of a balloon borne telescope can be maintained given adequate state data from a complement of sensors. Consequently, only generic attitude, rate, and acceleration sensors were assumed for this study. These assumptions include representative noise models.

3 SYSTEM DESIGN

The balloon system consists of a helium balloon, flight train, coarse azimuth pointer, gondola and instrument. The flight train is typically around 250 ft (76.2 m) long and consists of a parachute and a series of cables. The length of the parachute and cables coupled with the small distances between the cables result in large rotational compliance in the overall flight train. At the end of the flight train, the coarse azimuth pointer is connected to the gondola though cables and a spreader bar.

Kinematically, the system architecture utilizes an existing azimuth pointing system to coarsely control the azimuth of the entire gondola, on which is mounted an orthogonal pair of pitch and yaw gimbals for fine control of the telescope. Fig. 1 depicts the gimbal arrangement. The outer frame is suspended from the coarse azimuth pointer via 4 cables and is tilted 45° to allow the telescope to achieve elevation angles of 0-90°. Fig. 2 shows the total system, with the ancillary supporting items included. For purposes of clarity, solar panels are not shown.

The gimbals are articulated with direct drive brushless torque motors, taking advantage of their high motor constants (i.e., the ability of the motor to produce high torques with low power). This approach avoids the introduction of two deleterious non-linearities, namely, backlash due to gear trains and static friction due to brushes. It also allows for continuous pointing by making use of the attachment of the gondola to the flight train to absorb the momentum reacted from the telescope into the gondola. Electrical energy is replenished during the day via solar panels.

A key feature of the system is the hub design of the pitch and yaw gimbals. Static friction is eliminated by keeping the bearing shaft constantly rotating utilizing a small torque motor and planetary gear reduction box. The design goal was to keep the shafts rotating faster than the highest angular rate of the telescope while minimizing the power required. In order to minimize the residual secular dynamic bearing friction, the opposing gimbal shafts are rotated in opposite directions. These motors are run utilizing simple and reliable open loop control with a nominal shaft rotation rate of 1 rad/sec.

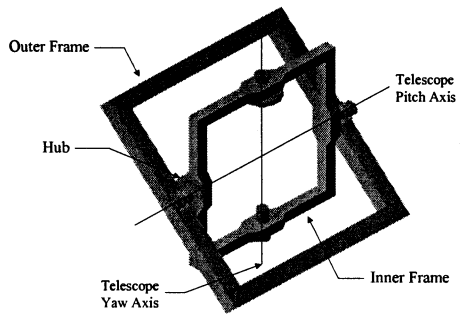

Fig. 1. Gimbal Diagram

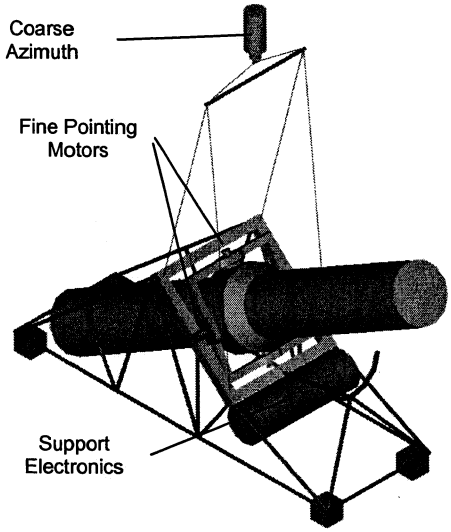

Fig. 2. System Diagram

Fig. 3 is a cross section of the bearing hub. The companion hub on the opposite side of the gimbal is identical except the torque motor that actuates the gimbal is not needed.

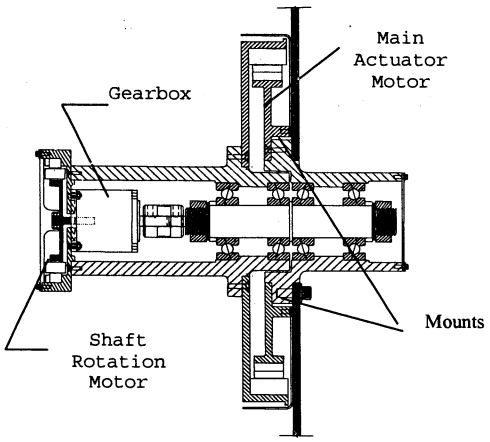

Fig. 3. Gimbal Hub Cross-Section

Operationally, the telescope will be caged during ascent and remain so until the acquisition sequence begins. The coarse azimuth controller will then rotate the gondola to the nominal target azimuth, which will be maintained throughout the observational period. The pitch and yaw axes will then be activated to bring the telescope to the target attitude. Nominally, there will be no rotation about the yaw axis and orthogonality is maintained between the pitch and yaw axes. This minimizes the cross coupling between these axes. Fine control on the pitch and yaw axes compensate for residual errors in the coarse azimuth control.

4 SYSTEM DYNAMICS

A detailed description of the system dynamics is provided in [6]. The basic ideas will be summarized here.

Gondola and flight train dynamics about the vertical (azimuth) axis are represented by a rotational linear mass-spring-damper combination in line with the coarse azimuth pointer. In the two other axes (pitch, roll) the gondola and flight train dynamics are represented by modal analysis of the pendulous modes. The instrument model was developed using Euler's equations, which include gyroscopic effects.

4.1 Yaw Axis Model (Mass-Spring-Damper)

The azimuth axis dynamics can be modelled as a set of spring-mass-damper equations with the coarse azimuth pointer included. From this model, a set of linear dynamics equations can be produced in the state-space form.

4.2 Roll and Pitch Axis Models (Modal)

The model of the flight train dynamics in the roll and pitch axes was developed using modal analysis. The flight train, consisting of the parachute, cable ladder, coarse azimuth pointer, and gondola was discretized into 10 elements. One element was used for the gondola and one for the chute release. Four elements each were used to model the parachute and the cable ladder. Masses were represented as point masses at the end of each element. The only difference in modelling between the roll and pitch axes is the configuration of the cabling between the coarse azimuth pointer and the gondola. By the design configuration, the pitch axis stiffness is significantly greater than the roll axis stiffness.

A Lagrangian analysis of the system was completed to derive the equations of motion. The modes of the system can be deduced from the eigenvalues and eigenvectors of the system. The results of this analysis for the first ten modes in both the roll and pitch axes are provided (Table 1), using a generalized inertia of 1 sl-ft^2 (1.356 kg-m^2). Ten modes were chosen to reduce the error in discretization.

4.3 Instrument Model

The equations of motion of the instrument in the body frame are derived from the kinematics of the pitch-yaw gimbal mount and Euler's equations of motion. The kinematics of the body axes are defined by the pitch and yaw angles (α, β).

Table 1. Modal Data

	Roll Axis		Pitch Axis	
Mode	f (hz)	K (N-m/rad)	f (hz)	K (N-m/rad)
1	0.027	0.039	0.055	0.160
2	0.173	1.594	0.365	7.111
3	0.502	13.470	0.686	25.150
4	0.756	30.579	0.958	49.096
5	1.103	65.146	1.113	66.295
6	1.396	104.254	1.396	104.323
7	2.117	239.965	2.128	242.386
8	2.800	419.477	2.801	419.973
9	4.000	856.344	4.001	856.787
10	5.105	1394.800	5.105	1394.879

4.4 Motor Models

Both the coarse azimuth pointer and the fine pointing actuators have been modelled as direct drive DC torque motors as given in Eq. 14. There are three components to the torque output of the motor: the ideal torque asked for by the controller, back EMF losses, and motor damping due to rotational eddy losses [2].

4.5 Bearing Models

Each gimbal consists of two sets of angular contact bearings - one set on each side. Kinetic bearing friction can be described by the sum of two components, the load-dependent (M_1) and load-independent (M_0) moments. The value of M_0 is a function of the type of bearing and lubricant as well as the angular velocity.

Since the load-independent moment exists for each bearing, it is multiplied by the number of bearings in the set (n) and added to the sum of the load-dependent values for each bearing to get the total bearing friction for that set [3].

The static bearing friction moment can be estimated to be twice the value of the load-dependent moment. For slow moving bearings, as is the case in this application, the value of M_0 is very small when compared with M_1. Therefore, the static friction is nearly twice the value of the kinetic friction.

5 COARSE AZIMUTH CONTROL

The coarse azimuth controller model is based on the Solar Pointing System (SPS) developed at NASA Wallops Flight Facility [4]. The SPS is a flight proven system consisting of a bearing-shaft arrangement actuated by a DC torque motor. The SPS control law implements a Proportional-Integral-Derivative (PID) controller with an Inner Velocity Loop (IVL). SPS controller output is in the form of pulse width modulation (PWM) and includes a 1 Hz filter. From the SPS controller block diagram, the control law can be derived (Fig. 4).

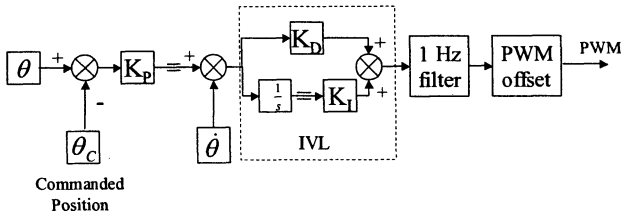

Fig. 4. SPS Coarse Azimuth Control Law

It is important to note the inclusion of measured rate in the feedback of the SPS controller, which is accomplished using an analog rate sensor. The SPS has been proven to maintain azimuth pointing of a large gondola within 1 degree [5].

6 FINE POINTING CONTROL

The control laws for the two fine pointer controllers include PID controls with acceleration feedback for enhanced disturbance rejection.

6.1 PID Fine Pointing Control

The PID controllers for both the pitch and yaw gimbal axes use angular position and rate sensor data. The output of the PID controller is a commanded torque T_{PID} (Fig. 5).

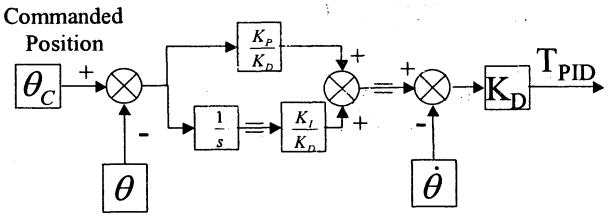

Fig. 5. PID Fine Pointing Control Law

6.2 Acceleration Feedback

To enhance disturbance rejection, the PID fine pointing controllers are augmented with acceleration feedback (fig. 6), designated PIDA. When a torque is applied to the instrument, the measured acceleration gives insight into the type and magnitude of any disturbances on the system. The acceleration feedback is compared to the previous commanded torque from the PID controller and the difference is added to the PID torque. This, in effect, attempts to counteract the disturbances on the system before they can integrate to position error.

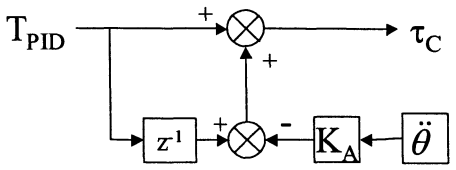

Fig. 6. Acceleration Feedback Control

The accelerometer is modelled as a 2nd order system. The acceleration gain, K_A, was initially chosen to be the instrument inertia in the particular control axis. It was found however, that this case is marginally stable. In fact, even a very little amount of accelerometer feedback can help in disturbance compensation. The acceleration gain for the simulated controller in both axes was chosen to be one half of the instrument inertia. This yields 6dB of gain margin.

High-resolution angular acceleration data for control feedback can be attained using linear accelerometers by taking advantage of the long instrument baseline as shown in Fig. 7.

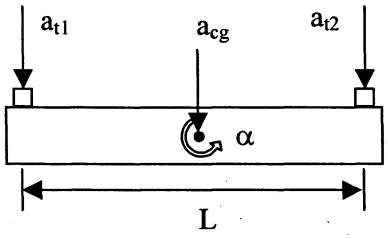

Fig. 7. Accelerometer Placement

$$a_{t1} = \alpha\left(\frac{L}{2}\right) + a_{cg}\ , \quad a_{t2} = -\alpha\left(\frac{L}{2}\right) + a_{cg} \quad (17)$$

$$\alpha = \frac{a_{t1} - a_{t2}}{L} \quad (18)$$

7 LINEAR ANALYSIS RESULTS

Stability of the yaw and pitch controllers was examined by linearizing the models around the most difficult pointing situation. The stability analyses of both axes are presented with the continuous PID controllers only.

7.1 Yaw Axis Stability Analysis

For the azimuth axis, a linearized MIMO model in state space form was computed based on the derived non-linear equations of motion. The coarse azimuth compensator gains were taken from the SPS nominal design. The initial fine pointer gain values used were K_P = 34000 ft-lb/rad (46098 N-m/rad), K_I = 51000 ft-lb/rad/sec (69147 N-m/rad/sec) and K_D = 17000 ft-lb-sec/rad (23049 N-m-sec/rad). With inspection of the Bode Diagrams (Fig. 8), the stability margins are:

Lower Gain Margin = 13.85 dB
Phase Margin = 69.34 deg

These yaw axis stability margins are well above the general robust stability criteria of 6dB and 30 deg. The system time response to an impulse input (Fig. 9) shows a very well damped system with a high response frequency and a 2% settling time around 2 seconds.

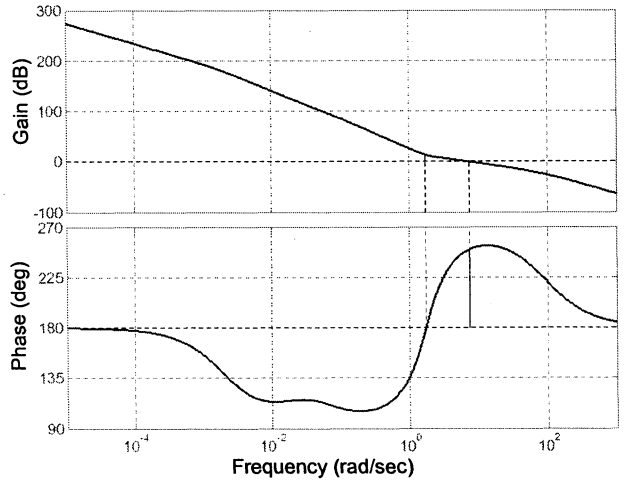

Fig. 8. Yaw Axis Frequency Analysis

7.2 Pitch Axis Stability Analysis

For the pitch axis, a linearized SISO model in state space form was computed based on the derived linear modal equations. Gain values were identical to those used for the yaw axis and Bode diagrams (Fig. 10) show the stability margins to be similarly robust:

Lower Gain Margin = 13.69 dB
Phase Margin = 69.12 deg

The system time response to an impulse input (Fig. 11) shows a very well damped system with a high response frequency and a 2% settling time around 2.5 seconds.

7.3 Inclusion of PIDA Control

The results of the PIDA controller on the linear yaw dynamics are shown in Fig. 12. Both a continuous PID and a discrete (20Hz) PIDA controller are shown. No discrete PID controller is shown because of the response similarity to a continuous PID. For both controllers, the linear system is subjected to a 1 ft-lb disturbance for a duration of 0.2 sec. The continuous PID controller has a slower response to the disturbance and thus allows the acceleration to integrate into a much larger position error. The discrete PIDA controller acts on the disturbance faster and cuts the total position error by 50%. The PIDA controller also

inputs less torque to the system, therefore requiring less power. This result was demonstrated in multiple disturbance cases.

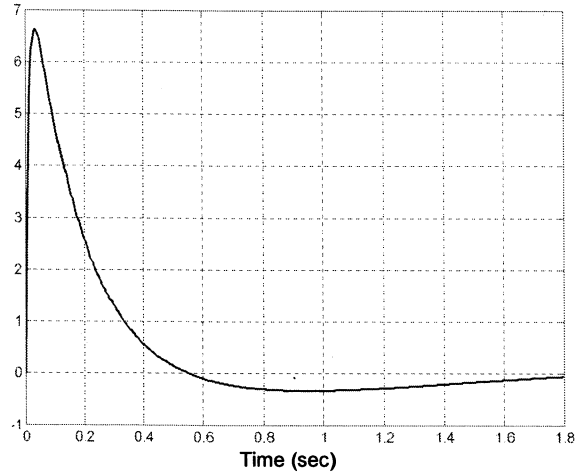

Fig. 9. Yaw Axis Impulse Response

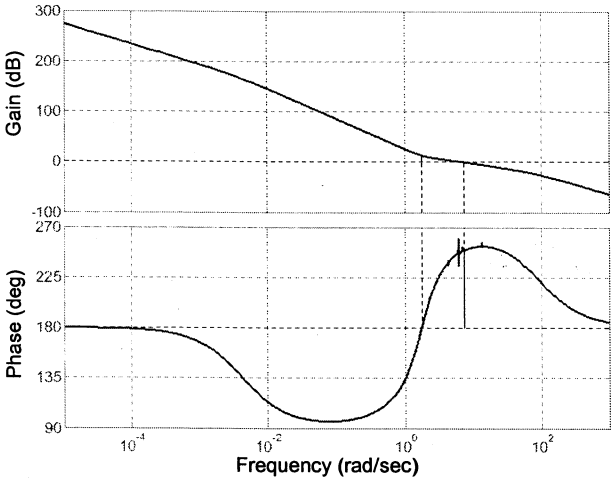

Fig. 10. Pitch Axis Frequency Analysis

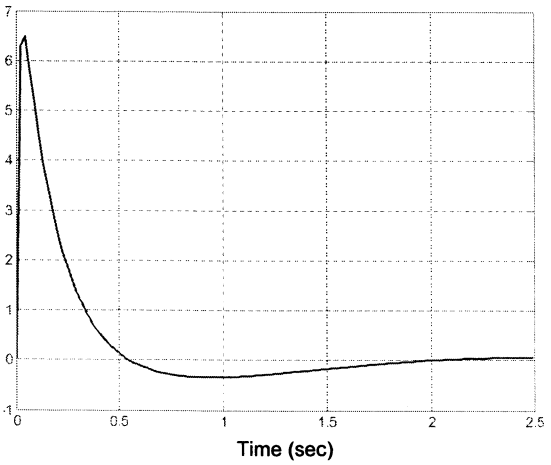

Fig. 11. Pitch Axis Impulse Response

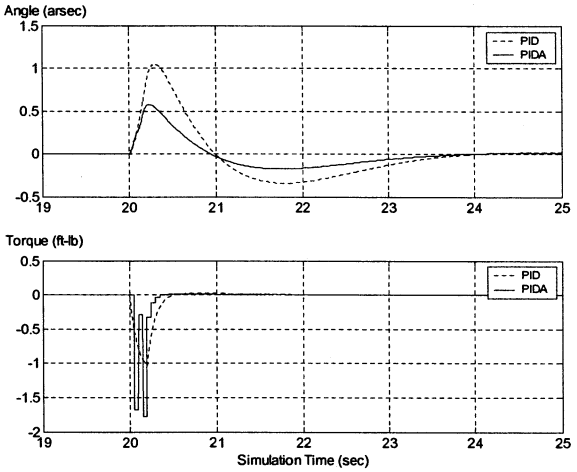

Fig. 12. Yaw Axis Linear Model Controller Comparison

8 SIMULATION RESULTS

The simulation includes system non-linearities such as signal clipping, coulomb friction, and gyroscopic cross-coupling of the gimbal axes. Signal clipping includes rate and integral clipping, maximum motor torques and controller torque clipping. All simulation runs were completed with the three controllers (coarse azimuth, pitch, yaw) running at 20 Hz.

To demonstrate the efficacy of rotating the gimbal shafts, results from the non-linear simulation were viewed for both the rotating and non-rotating conditions in the yaw axis. The results indicate that if the shafts are not rotated, it is not possible (with the current controller) to maintain pointing under the desired 1 arcsecond (Fig. 13). However, when the shafts are rotated, the pointing ability of the system is greatly increased and the 1 arcsecond target is maintained (Fig. 14).

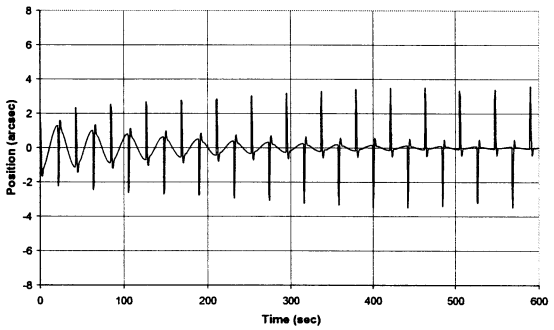

Fig. 13. Yaw Axis Simulation Results, Nonrotating Shafts

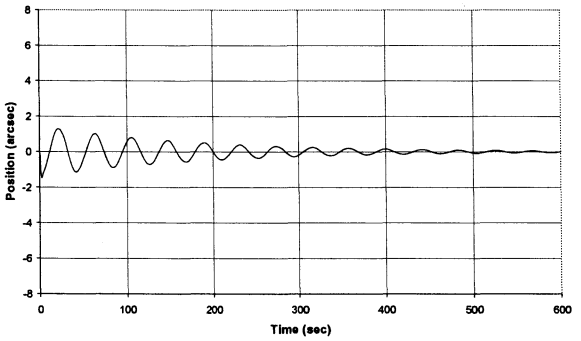

Fig. 14. Yaw Axis Simulation Results, Rotating Shafts

This holds true even when the shafts are rotated in the same direction, the resulting secular torque being easily compensated by the integrator. The low frequency oscillations in both figures are from the coarse azimuth pointer limit cycle of about 3 degrees during initial target acquisition. This is intentionally induced in order to stimulate controller activity in the simulation.

System performance was examined with parametric simulations varying the type, magnitude, and frequency of disturbances. High and low frequency oscillatory disturbances, as well as step and pulse disturbances were tested. Simulations included disturbances to both the instrument and the gondola. The yaw axis proved the more challenging axis, as was initially expected and verified by the linear analysis. This is due to the relatively high compliance in the flight train cables and the existence of dual controllers.

Credible values of the frequencies and magnitudes were determined analytically and based on previous balloon flight data. The magnitude of the disturbances was chosen to be greater than those considered realistic to verify stability and performance margins. In all simulation test runs, the coarse azimuth pointer is started 30 degrees from the target to stimulate its limit cycle and introduce additional disturbances into the yaw axis. For the results given, the disturbances are applied directly to the instrument. Realistically, disturbances from the flight train and gondola motion would only affect the instrument through the gimbal hubs, thus the disturbances given are worse than realistically expected.

The first results shown are for a 1 ft-lb (1.356 N-m) step disturbance on the pitch and yaw axes (Fig. 15). In both axes, the disturbance is quickly damped out and the integrator returns the system to nominal pointing.

The first oscillatory disturbance is a low frequency oscillation (0.05Hz) in the pitch and yaw axes close to the frequency of the 1st pitch axis pendulous mode (Fig. 16). The second is a high frequency oscillation (1.5Hz) in the pitch and yaw axes close to the bandwidth of the system (Fig. 17).

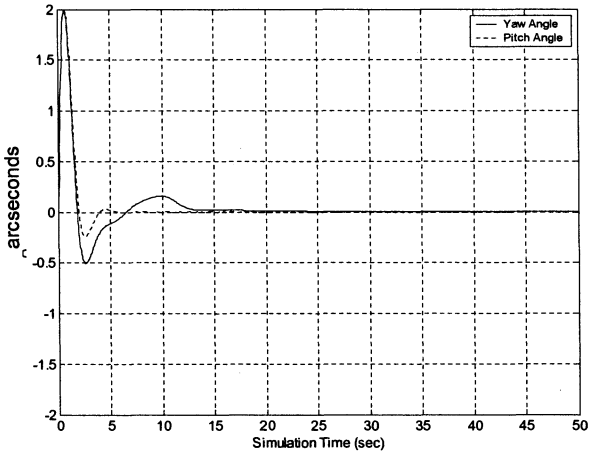

Fig. 15. Simulation Response to 1 ft-lb Step Disturbance in Pitch and Yaw

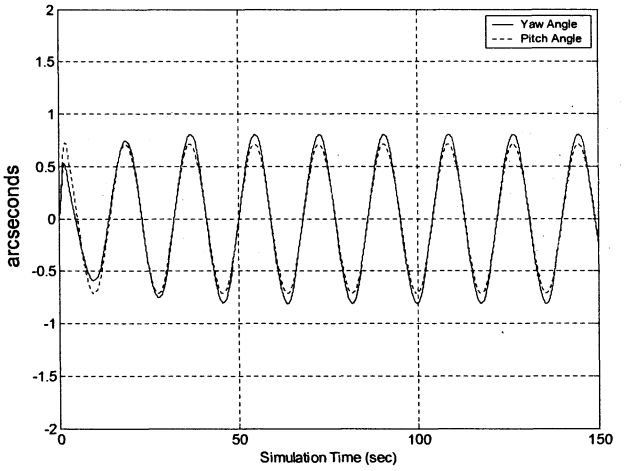

Fig. 16. Simulation Response to 1 ft-lb Low Frequency (0.05 Hz) Disturbance in Pitch and Yaw

Both test runs indicate the ability of the system to respond to disturbances, with magnitudes higher than considered realistic, and maintain targeted pointing. In the low frequency test, the system maintains less than one arcsecond, indicating a good disturbance rejection ability. As an indicator of the low power design of this control system, the approximate required shaft power for the gimbal motors to maintain this pointing, even under these unrealistically high disturbances, is 1.4 watts per motor. Additional power would be required to rotate the hub shafts, power the course pointer and power the electronics chosen for implementation. In the high frequency test, sub-arcsecond response is also maintained even though the disturbance is above the

bandwidth of the system. The system gain at this frequency is –2.7 dB, which is desirable for noise rejection.

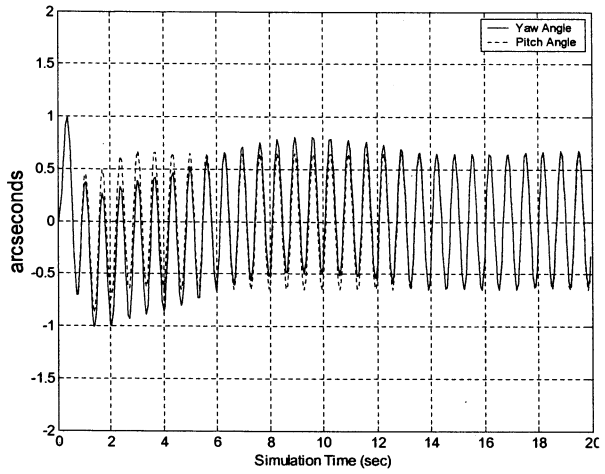

Fig. 17. Simulation Response to 1 ft-lb High Frequency (1.5 Hz) Disturbance in Pitch and Yaw

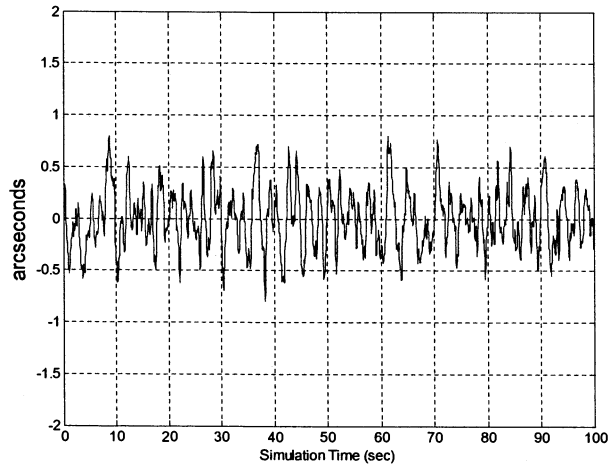

Fig. 18. Yaw Axis Simulation Response to Sensor Noise

Another parametric run was completed using sensor noise. White noise was introduced to various sensors to determine the system's reliance on sensor information. Positional noise has a direct effect on pointing ability and displaying the results of positional noise runs is unnecessary. In the case of a PIDA controller, however, both rate sensor and accelerometer noise will be present. Simulation runs were completed in the yaw and pitch axes using 2 arcsecond/sec rate noise and 20 arcsecond/sec^2 acceleration noise The results for the two axes are similar, so only the yaw axis is shown (Fig 18). With this level of noise, the controller is still able to maintain pointing in the desired envelope. Similar tests can be completed to deduce the required sensor accuracy to achieve any pointing requirement.

9 DEMONSTRATION PROTOTYPE DESIGN

A demonstration prototype of the above system was assembled from Commercial Off-the-Shelf (COTS) hardware. Details of the COTS items used are provided for each component. The items were chosen to best fit within the system design constraints. The system was implemented without the coarse azimuth pointer due to lack of SPS availability during testing. Also, although accelerometers were procured for testing, the required A/D resolution was not available from the COTS hardware procured. Therefore, the system was tested in the PID mode only.

9.1 Mock Instrument

The instrument payload was simulated using a "dead weight" mock instrument. Mass properties of the mock telescope were selected to chosen to match the size and weight of large Aries class telescopes. Stiffness was also important in the mock instrument selection. Thus, a 24 ft (7.3m) long steel square beam with 10 inch (0.25m) sides was chosen. The beam's mass was 1500 lb (680 kg). The sensors, batteries, and cabling were all distributed on the mock instrument so as to maintain balance about the gimbal hubs. Additional small weights were placed at the ends of the beam to assist in balancing, if necessary.

9.2 Pitch-Yaw Gimbal Mount

The Pitch-Yaw gimbal mount and the gimbal hubs were the only specially fabricated elements of the prototype. The gimbal frames were made out of aluminium tubing and the the hub components were bored from aluminium stock.

The shaft rotation motors were small , gear boxes, and bearing sets were all selected from stock equipment. The availability of these items was taken into consideration in the design. The two drive motors used were Kollmorgen Brushless DC Torque Motors, Model BM-11303. A COTS digital motor driver was used with resolver feedback from the hubs for motor commutation.

9.3 Sensors

For this test, a three-axis gyro package was used for both rate and position information. Mock instrument rates were output from the gyros and digitally integrated to determine the instrument position. High precision linear accelerometers are attached to the ends of the mock instrument for use in calculation of angular acceleration.

9.4 Command and Data Handling

A data acquisition board in a desktop computer received all of the sensor signals in analog form. The desktop computer runs the control software and calculates the commands. These commands are sent to the motor drivers to actuate the motors. The desktop computer running the control software sends all measured and calculated data to another desktop for logging and display.

9.5 Gondola Setup

For the demonstration prototype, the gondola consisted of a series of weights attached to the outer gimbal frame and distributed to match the typical inertia of a balloon gondola.

9.6 Hangtest Setup

The gondola was suspended using chains from four corners of the structure to a spreader bar. The spreader bar was connected to a bridge crane through two nylon slings.

10 TESTING RESULTS

The system was hung from the bridge crane and performance tested. During the tests, the system demonstrated sub-arcsecond pointing. A data sample from one jitter test shows the system pointing performance (Fig 19). During this test, the gondola was swinging at an amplitutde of +/-1 degrees. Statistical analysis of the data demonstrates the system jitter accuracy. Figure 20 shows a pitch-yaw plot with the data points over the test run. There are four circles displaying the statistical data as well as the 1 arcsecond goal. As can be seen by the figure, the 3-sigma system jitter was less than 0.75 arcseconds.

In addition to jitter tests, multiple disturbance tests were executed. Pendulous disturbances were introduced to the gondola by pushing on the gondola structure. A torsional disturbance was introduced to the gondola by rotating the gondola structure roughly 15 degrees and releasing, allowing the hang test flight train to impart a restoring torque. The pointing system recovers from the initial large restoring torque quickly, and settles into a bounded oscillatory motion of approximately 1 arcsecond in magnitude (Fig 21). Axial disturbances on the gondola are introduced by pushing the gondola to induce swinging. The system recovers from large amplitude swinging as well (Fig 22). Another test was executed where a 1 lb (0.45 kg) weight was dropped from 1 ft (0.30 m) onto the gondola at 460 seconds. In this test, the system barely even sees the disturbance (Fig 23). Disturbances can only get to the mock instrument through the rotating bearings, and this disturbance hardly propagated through the hubs.

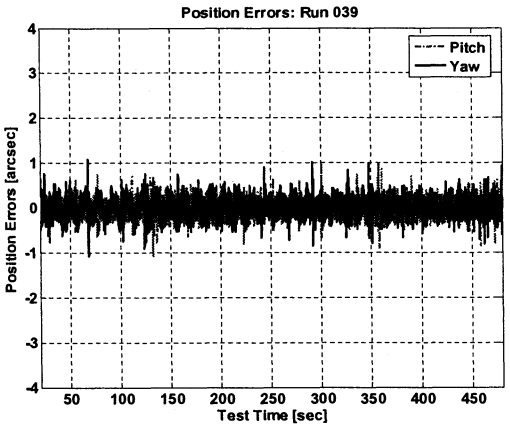

Fig. 19. Time-history of Sample System Jitter Test

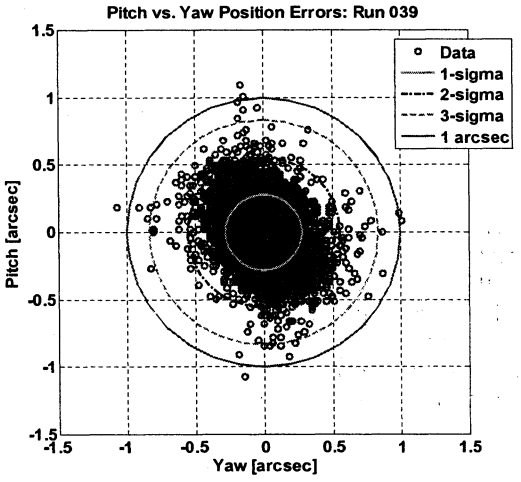

Fig. 20. Sample System Jitter Test Statistical Data

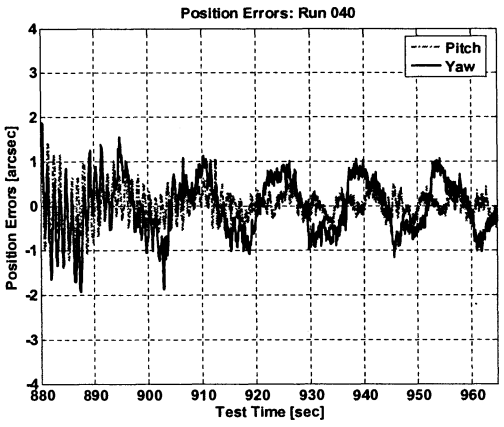

Fig. 21. System Response to Torsional Disturbance

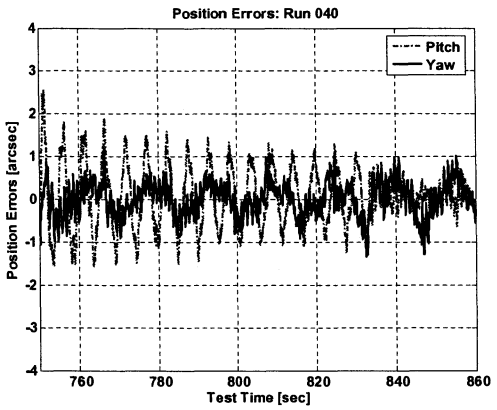

Fig. 22. System Response to Axial Disturbance

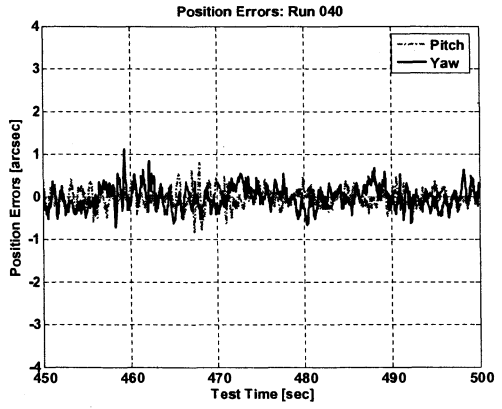

Fig. 23. System Response to Step Disturbance

11 CONCLUSIONS

Suspension of a telescope from a balloon subjects the instrument to torques that create significant challenges to fine pointing. However, the same source of these control challenges, namely the attachment to the gondola and flight train, can be harnessed to provide solutions that meet the challenge. The results of this study indicate that the proposed system is capable of adequately rejecting disturbances larger than those considered realistic. It is also shown that the proposed control strategy can be made robustly stable with significant design margins. A demonstration prototype of the designed system was built using COTS hardware that demonstrated sub-arcsecond pointing in an environment similar to flight. Finally, we conclude that sub-arcsecond pointing stability can be achieved for a large balloon borne instrument pointing at an inertial target.

12 REFERENCES

1. United States Committee on Extension to the Standard Atmosphere, "U.S. Standard Atmosphere, 1962," U.S. Government Printing Office, 1962.

2. Inland Motor Specialty Products Group, "Direct Drive DC Motors," Kollmorgen Corporation, 3rd Printing 1985.

3. SKF Group, "SKF General Catalog," Printed by Command Web Inc., 1991.

4. A. V. Hanagud, J. M. Simpson, R. J. Lanzi, W. R. Dufrene Jr., and S. A. Bailey, "A Solar Pointing System for the Long Duration Balloon Missions", AIAA International Balloon Technology Conference, San Francisco, CA, June 1997.

5. Lanzi, R. J., "LDB Rotator Test Flight Summary", Internal Memorandum, NASA/GSFC/WFF, 1997.

6. P. Ward, K. DeWeese, "Balloon Borne Arcsecond Pointer Feasibility Study," 16th ESA Symposium on European Rocket and Balloon Programmes and Related Research, Proceedings of, June 2003, pp. 197-205